Integrated photonic crystal waveguides on silicon-on-sapphire for chemical sensing in mid-infrared

Yi Zou,[1,*] Swapnajit Chakravarty,[2,*] Xiaochuan Xu,[2] and Ray T. Chen [1, 2, *]
[a]Dept. of Electrical and Computer Engineering, University of Texas, 10100 Burnet Road Bldg. 160, Austin, TX, USA 78758;
[b]Omega Optics Inc., 8500 Shoal Creek Blvd., Austin, TX 78757

ABSTRACT

We experimentally demonstrate transmission characteristics of a W1 photonic crystal waveguide in silicon on sapphire at mid infrared wavelength of 3.43 μm. Devices are studied as a function of lattice constant to tune the photonic stop band across the single wavelength of the source laser. The shift in the transmission profile as a function of temperature and refractive index is experimentally demonstrated. In addition to zero transmission in the stop gap, high transmission was observe for the characteristic of the waveguiding behavior of photonic crystal line defect modes.

Keywords: silicon photonics, mid-infrared, photonic crystal waveguides.

*yzou@utexas.edu, swapnajit.chakravarty@omegaoptics.com, raychen@uts.cc.utexas.edu;
phone 1 512-471-4349; fax 1 512-471-8575;

1. INTRODUCTION

Silicon has been the material of choice of the photonics industry over the last decade due to its easy integration with silicon electronics as well as its optical transparency in the near-infrared telecom wavelengths. In recent years, photonic devices on chips are increasingly being used for chemical and biological sensing. Ring resonators [1], photonic crystal waveguides (PCWs) [2], photonic crystal (PC) microcavities [3] operating at 1.55 μm have been employed for biosensing. Optical biosensors can be theoretically designed for operation at any wavelength after taking into consideration the absorbance of water based biological media. In contrast, chemicals are best recognized by their unique wavelength specific optical absorption signatures. Slow light in PCWs [4] and PC slot waveguides [5, 6] has been used to reduce the optical absorption path length and achieve high detection sensitivity in on-chip optical absorption spectroscopy for the selective detection of volatile organic compounds [5] and greenhouse gases [6] based on unique analyte absorption signatures in the near-infrared (near-IR). It is common knowledge that in contrast to the near-infrared, the mid-infrared (mid-IR) wavelengths offer at least two orders of magnitude larger absorption cross-sections than the near-IR. Silicon is optically transparent over the entire mid-IR till about 8μm [7]. Hence, PCWs and PC slot waveguides in silicon-on-insulator (SOI) (till 3.7μm), silicon-on-sapphire (SoS) (till 5.5μm) and free-standing silicon membranes (till 8μm) can serve as the ideal platform for highly sensitive optical absorption spectroscopy on chip. Strip [8-11] and slot waveguides [12] have been demonstrated by several groups in the mid-IR in silicon on both SOI and SoS. In spite of available material platforms and laser sources in the mid-IR, PC research in the mid-IR has been limited by the non-availability of appropriate tunable laser sources that can characterize the entire PC transmission bandwidth [13, 14]. Optical parametric oscillators (OPOs) provide a relatively expensive and bulky option using free-space optics for optical coupling into mid-IR optical devices, and untenable for any realistic sensing system outside the lab [13]. Previously PC microcavities and PCWs have been demonstrated in free-standing silicon membranes in SOI in the mid-IR wavelengths [13, 14].

In this paper, we present the first demonstration of photonic crystal waveguide (PCW) characteristics in SoS at the mid-IR wavelength 3.43 μm of our fixed wavelength interband cascade laser (ICL). We demonstrate that by good control of device fabrication and device parameter engineering, PC waveguiding properties can be adequately determined in mid-

Silicon Photonics X, edited by Graham T. Reed, Michael R. Watts, Proc. of SPIE Vol. 9367,
93670T · © 2015 SPIE · CCC code: 0277-786X/15/$18 · doi: 10.1117/12.2080266

IR PC devices to facilitate the accurate design of mid-IR PC sensors. The SoS platform provides a more rigid option for photonic sensing applications in the mid-IR compared to free-standing silicon membranes in SOI.

2. DEVICE WORKING PRINCIPLE

The principle of operation of optical absorption spectroscopy is governed by the Beer–Lambert law. According to this law, the transmitted intensity I is given by

$$I = I_0 \times \exp(-¥\sim L) \tag{1}$$

where I_0 is the incident intensity, α is the absorption coefficient of the medium, L is the interaction length, and γ is the medium-specific absorption factor determined by dispersion-enhanced light–matter interaction. For various applications, L must be large to achieve high sensitivity since γ=1. In addition, from perturbation theory

$$¥ \propto f \times \frac{c/n}{v_g} \tag{2}$$

where c is the speed of light in free space, v_g is the group velocity in the medium, and n is the refractive index of the medium [15]. The term f is the filling factor denoting the relative fraction of optical field residing in the analyte medium. Group velocity v_g is inversely proportional to the group index n_g.

Mid-infrared covers most characteristic absorption bands of various organic and inorganic compounds that contain the molecular fingerprints, it has become very attractive for sensor applications. Compared with near-infrared spectroscopy, most of the chemical bonds have much stronger absorption peaks in mid-infrared than near-infrared, so by moving from near-infrared to mid-infrared the sensitivity of spectroscopy can be greatly enhanced by several orders [16].

At the same wavelength, since absorption coefficient ~ does not change, the way to improve sensitivity while keeping the same device length L is to increase γ. As shown in Eq. 2, increase f or n_g or both of them two can lead to increase γ and hence enhance sensitivity. Slot waveguides have demonstrated in near-infrared that it can significantly increase the electric field intensity in the narrow slot which is filled with low index material. The enhancement can be around 10 times strong than conventional waveguide [17]. Photonic crystal waveguide has also been demonstrated in near-infrared that it can slow down the group velocity up to 100 [18]. These two devices provide the potential methods to increase γ and hence sensitivity [19]. By considering these two factors theoretically we can expected strip waveguide, slot waveguide, photonic crystal waveguide and slotted photonic crystal waveguide on the same chip will have optical absorbance increases in order as follow: (a) strip waveguides which has n_g~3, (b) slotted strip waveguides which has n_g~3 and f~10 since the intensity of light in a low-index slot is significantly enhanced compared to strip waveguides, (c) PCWs which has n_g~100, and (d) slotted PCWs which has f~10 and n_g~100 for a combined factor of ~1000.

Hence, due to an increase in ~ in Eq. 1, together with the device enhancements from Eq. 2, mid-infrared spectroscopy can be expected to have a larger sensitivity in absorption spectroscopy than in the near-infrared.

3. DEVICE DESIGN

The device comprises a conventional W1 PCW with a single missing row of holes along the dJh direction in a hexagonal lattice of air holes in silicon. Fig. 1(a) shows the simulated transmission spectrum of a W1 PCW with lattice constant a=845 nm, radius of air holes r= 0.25a and height of silicon slab h=0.69a obtained by three-dimensional (3D) finite difference time domain (FDTD) simulation. Refractive indices of silicon and sapphire were considered as 3.429 and 1.7 respectively. A distinct transmission band edge is observed at-ª=3.445 μm. A conventional experimental demonstration of the transmission spectrum would simply comprise sweeping the wavelength range with a tunable spectrum and detector, or spectral identification via a spectral analyzer and a broadband source. However, it is also possible to characterize the PCW transmission characteristics by careful control of design and fabrication, and sweeping the lattice constant a. Fig. 1(b) shows a set of FDTD simulations of a W1 PCW with different lattice constant a=830 nm, 840 nm, 845 nm, 850 nm, 860 nm, 870 nm and 890 nm. The radius r was kept fixed at 0.25a. The height of the silicon

device layer according to wafer specifications is 600±60 nm. In this work, the height of the silicon device layer was determined to be h=585 nm from ellipsometry. The h/a of the silicon slab was calculated accordingly for each lattice constant. The wavelength spectrum of our Fabry-Perot ICL is shown by the dashed black line.

There is a group index mismatch between input strip waveguide and the PCW which will reduce the coupling efficiency, hence in order to overcome this problem we design a group index taper. Light is guided in and out of the PCW by strip waveguides with PC group index taper to enable high coupling efficiency into the slow light guided mode [20, 21]. Fig. 2 shows the dispersion diagram of the W1 PCW obtained by 3D plane-wave expansion simulation. Refractive indices of silicon and sapphire were considered as 3.429 and 1.7 respectively. Fig. 1(b) indicates that the ICL emission will propagate in the high group index regime in devices with a=845 nm. Fig. 2 is thus calculated with a=845 nm. The dispersion diagram shows the guided mode (in red) separated from the dielectric band by a stop gap. The light line for sapphire is superimposed. The PC group index taper is created by gradually tapering down the width of the PCW from the interface between the strip waveguide and PCW over 8 lattice periods from W1.07 to W1. W1.07 indicates that the width of the PCW at the onset of the taper is $1.07\times\sqrt{3}a$. The red dashed plot in Fig. 2 shows the dispersion of the guided mode when the PCW is W1.07. Two dashed blue lines are drawn on the dispersion plots of the guided mode at the representative frequency a/λ=0.246. The slope of the lines ω/k gives the group indices (8 and 30 respectively) for W1.07 and W1 PCW, where k is the wavevector and ω is the frequency. Hence instead of coupling light from the strip waveguide to the W1 PCW at a group index n_g=30 at a/λ=0.246 in Fig. 2, group index taper engineering results in light coupled from the strip waveguide into the PCW at n_g=8. It has been shown in the near-IR that such group index engineering reduces Fresnel reflection losses that would otherwise show significant fringe patterns in the PCW guided mode transmission spectrum [20, 21].

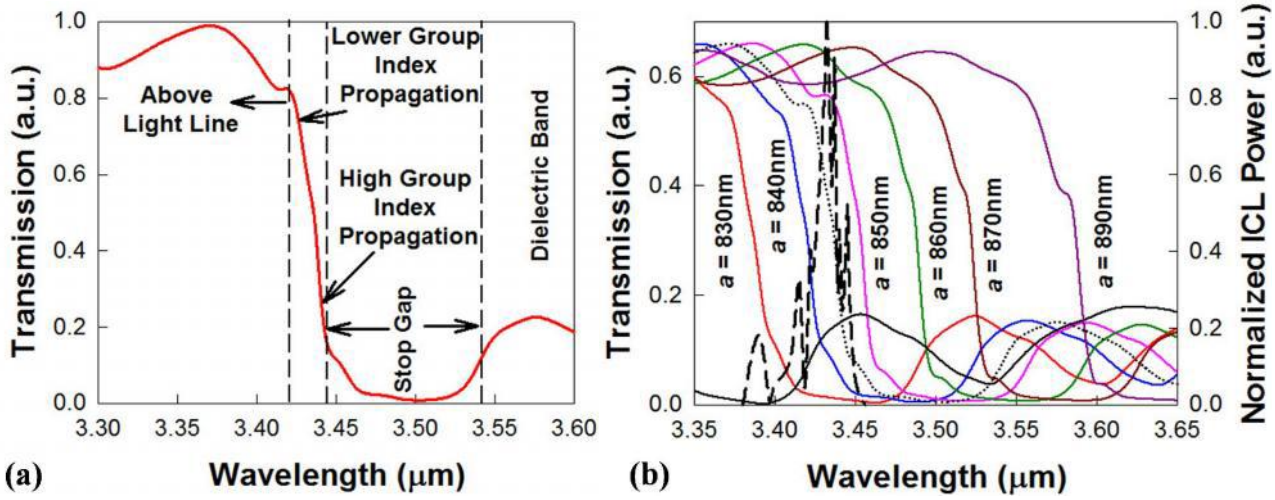

Fig. 1. (a) 3D FDTD simulation of a short W1 PCW in silicon-on-sapphire for operation at 3.43 μm with a=845 nm. The different parts of the transmission spectrum are indicated. (b) Set of 3D FDTD simulations of short W1 PCWs with different lattice constants a. Simulation for a=845 nm is indicated by the dotted black plot. The output spectrum of our source ICL is indicated by the dashed black plot (right axis).

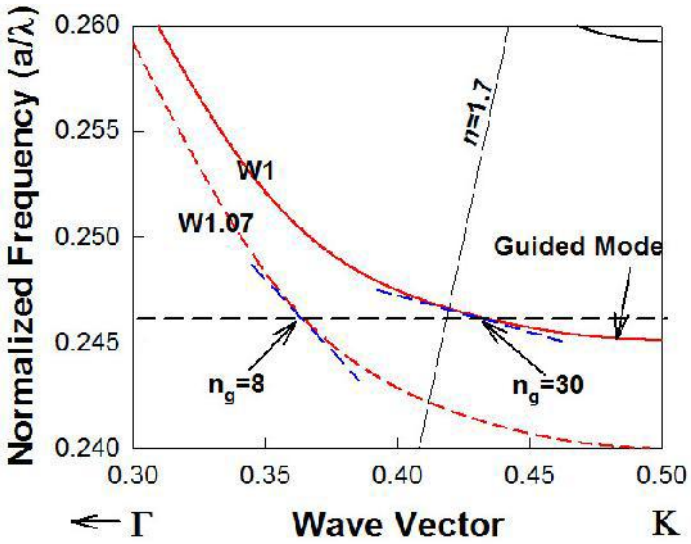

Fig. 2. 3D plane wave expansion simulation of the dispersion diagram of a silicon W1 PCW on sapphire substrate with air top cladding. The red dashed line indicates the PCW dispersion at the interface between silicon strip waveguide and W1.07 PCW. The reduced group index at the interface is indicated by the lesser slope (dashed blue lines) at a representative frequency a/λ=0.246. Sapphire light line is superimposed.

4. DEVICE FABRICATION

Devices were fabricated using a combination of electron beam lithography and inductively coupled plasma etching. The process started from a SoS platform with 585 nm silicon device layer on a 500 µm thick sapphire substrate. The fabrication flow is shown in Fig. 3. A 140 nm silicon dioxide layer was first deposited on top of silicon layer using plasma enhanced chemical vapor deposition (PECVD) to serve as a hard mask for pattern transfer. All the components including grating couplers, strip waveguides, PCW were patterned in one step with JEOL JBX-6000FS electron-beam lithography tool. In order to ensure good control over the fabrication process, a thin conductive polymer (ESPACER) from ShowDenko chemicals was spin coated on the ebeam resist ZEP-520A, prior to ebeam lithography. After ebeam exposure, the devices was rinsed in DI water to remove the conductive polymer and then was developed in n-Amyl acetate (ZEP-N50) for 2 mins, and rinsed in isopropyl alcohol (IPA). The ebeam resist pattern was next transferred to silicon dioxide by reactive ion etching (RIE) using CHF_3 and O_2 at 400 V DC bias and 40 mTorr pressure for 8 mins. Following this, the pattern in silicon dioxide was transferred to silicon by inductively coupled plasma (ICP) etch using HBr and Cl_2 at 400 W ICP power, 200 W RF power, 10 mTorr pressure and 20 Torr Helium flow for backside cooling for 6.5 min. Finally, the chip was cleaned using Piranha for 15 min and followed with three cycles of Piranha/HF post-process treatment.

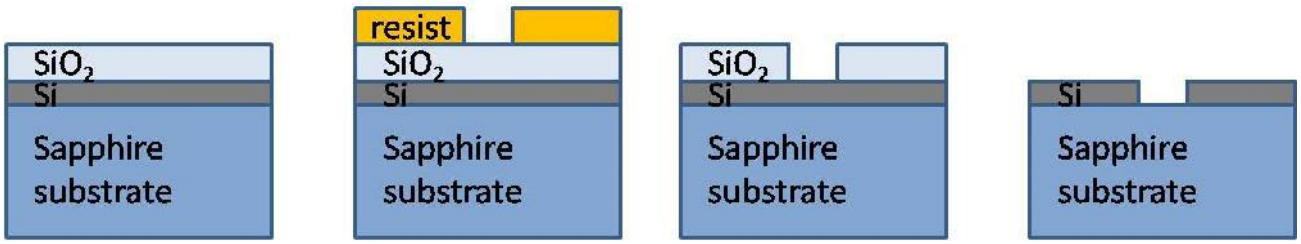

Figure 3: Fabrication steps of PCW (a) PECVD growth of oxide (b) E-beam Resist (ZEP-520A) patterning (c) Transfer of resist pattern to oxide by RIE using CHF_3 followed by resist strip (d) Transfer of pattern from oxide to Si by ICP in HBr and Cl_2.

SEM images of the fabricated devices are shown in Figs.4 (a)-(b).

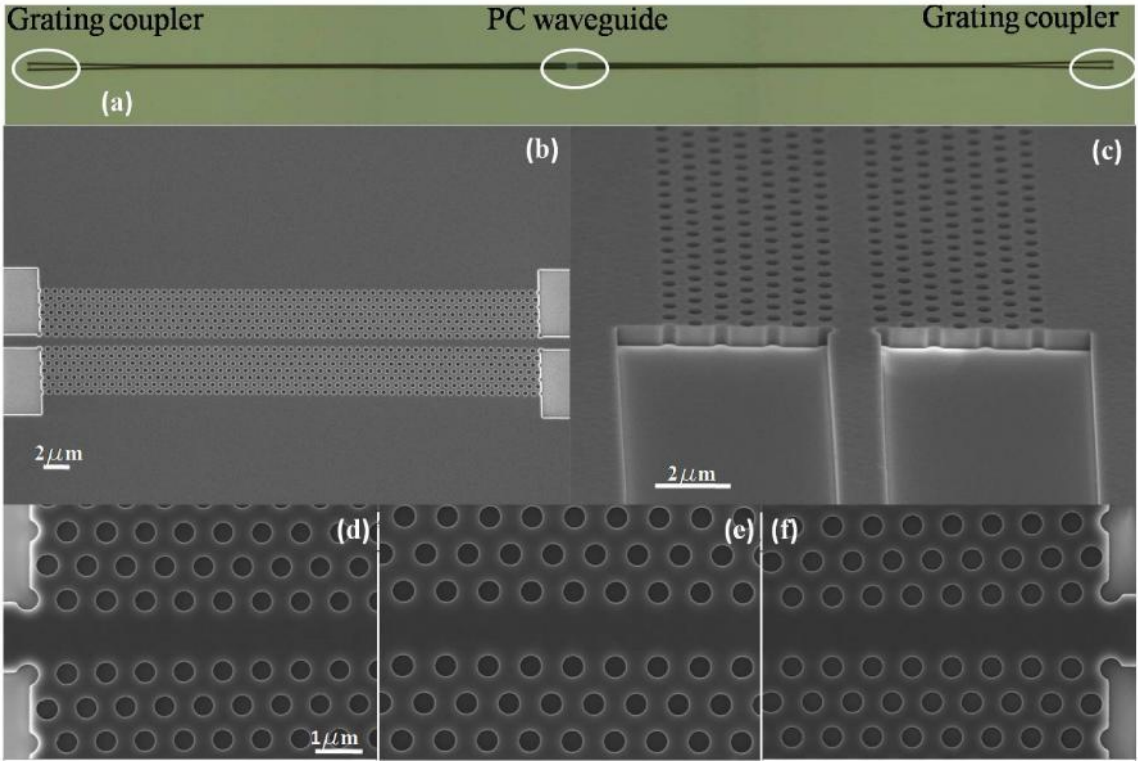

Fig. 4. (a) Microscope image of the device showing input and output SWGs and PCW. (b) Top view SEM image of PCW and (c) side view SEM image of the PCW at the PCW-strip waveguide interface. Magnified top view SEM images of (d) input taper (e) PCW and (f) output taper.

5. EXPERIMENTAL RESULTS

The light from the output SWG for PCW devices with several lattice constants but the same *r*/*a* is plotted in Fig. 5(a). The length of the W1 PCW is 50 μm. The plot is normalized with respect to the highest and lowest power observed versus lattice constant. It is observed that for *a* less than 845 nm, the output power from the devices is practically zero. Fig. 5(a) also plots the output power from the devices when immersed in tetrachloroethylene (C_2Cl_4). C_2Cl_4 is practically non-absorbing at 3.43 μm with a refractive index ~1.5 at room temperature. The absolute power measured by the photodetector is lower with C_2Cl_4 than with air cladding in Fig. 5(a) due to the lower modal confinement; however the normalized plot shows the transmission profile shifted to lower lattice constants. Fig. 5(b) plots the output power as a function of temperature for varying lattice constant. The temperature is varied from 25 ^oC to 60 ^oC. The normalized plot also shows a shift of the transmission profile to lower lattice constants, with increasing temperature.

At *a*=840 nm and lower, the probed wavelength of 3.43 μm is clearly within the photonic band gap; hence the transmitted power is zero. At lattice constants from *a*=845 nm to *a*=850 nm, the fixed wavelength ICL probes the W1 PCW guided mode at gradually decreasing group indices which translates experimentally to gradually increasing transmitted power. At a greater than 850 nm, the probed wavelength propagates above the light line and the transmitted power reaches a maximum for the short W1 PCWs.

When the cladding refractive index is increased from n=1 in air to n=1.5 in C_2Cl_4, the W1 PCW guided mode is shifted down towards the dielectric band in Fig. 2. All simulated curves in Fig. 1(b) are shifted to longer wavelengths. As a result, the 3.43 μm fixed wavelength source can be propagated through PCWs with smaller lattice constants. The phenomenon is experimentally observed by the shift of the transmitted intensity vs. lattice constant curves to shorter lattice constants. The effect of temperature can be similarly explained. Silicon has a positive temperature coefficient of refractive index at 3.43 μm [22]. An increase in temperature increases the silicon refractive index so that the W1 PCW guided mode is again shifted down in frequency in the normalized dispersion diagram in Fig. 2. As a result, the 3.43 μm source can be transmitted through PCWs with smaller lattice constants as temperature is increased, as observed in Fig. 5(b).

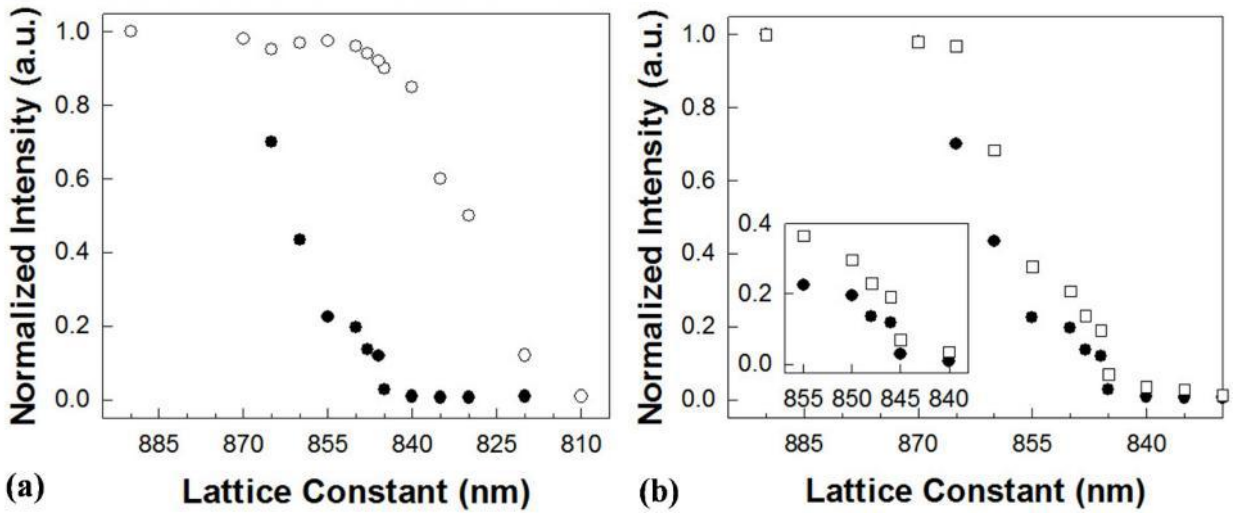

Fig. 5. (a) Normalized transmitted intensity through an air-clad W1 PCW in SoS with r=0.25a, as a function of a at ^{a}=3.43 μm plotted (a) in air (bold circles) and C_2Cl_4 (open circles) and (b) as a function of temperature at 25 ^{o}C (bold circles) and 60 ^{o}C (open squares). Insets magnify the data for devices between a=840 nm and a=855 nm.

6. SUMMARY

In summary, we demonstrated the propagation characteristics of PCWs in SoS in the mid-IR. By engineering the lattice constant, we experimentally demonstrated the transmission characteristics with a single wavelength source. Zero transmission in the stop band were experimentally observed. Our method enables the design of guided wave photonic structures, using miniature PC devices in the mid-IR, even in the absence of mid-IR tunable sources.

ACKNOWLEDGEMENTS

The authors acknowledge the National Science Foundation (NSF) for supporting this work under SBIR program (IIP-1127251).

REFERENCES

1. Iqbal, M., et al., *Label-free biosensor arrays based on silicon ring resonators and high-speed optical scanning instrumentation.* Selected Topics in Quantum Electronics, IEEE Journal of, 2010. **16**(3): p. 654-661.
2. Skivesen, N., et al., *Photonic-crystal waveguide biosensor.* Optics Express, 2007. **15**(6): p. 3169-3176.

3. Lai, W.-C., et al., *Silicon nano-membrane based photonic crystal microcavities for high sensitivity bio-sensing.* Optics Letters, 2012. **37**(7): p. 1208-1210.
4. Lai, W.-C., et al., *Multiplexed detection of xylene and trichloroethylene in water by photonic crystal absorption spectroscopy.* Optics Letters, 2013. **38**(19): p. 3799-3802.
5. Lai, W.-C., et al., *Photonic crystal slot waveguide absorption spectrometer for on-chip near-infrared spectroscopy of xylene in water.* Applied Physics Letters, 2011. **98**(2): p. 023304.
6. Lai, W.-C., et al., *On-chip methane sensing by near-IR absorption signatures in a photonic crystal slot waveguide.* Optics Letters, 2011. **36**(6): p. 984-986.
7. Soref, R., *Mid-infrared photonics in silicon and germanium.* Nature Photonics, 2010. **4**(8): p. 495-497.
8. Cheng, Z., et al., *Mid-infrared grating couplers for silicon-on-sapphire waveguides.* Photonics Journal, IEEE, 2012. **4**(1): p. 104-113.
9. Baehr-Jones, T., et al., *Silicon-on-sapphire integrated waveguides for the mid-infrared.* Optics Express, 2010. **18**(12): p. 12127-12135.
10. Li, F., et al., *Low propagation loss silicon-on-sapphire waveguides for the mid-infrared.* Optics Express, 2011. **19**(16): p. 15212-15220.
11. Spott, A., et al., *Silicon waveguides and ring resonators at 5.5 mu m.* Applied Physics Letters, 2010. **97**(21): p. 213501.
12. Zou, Y., et al., *Grating-coupled silicon-on-sapphire integrated slot waveguides operating at mid-infrared wavelengths.* Optics Letters, 2014. **39**(10): p. 3070-3073.
13. Reimer, C., et al., *Mid-infrared photonic crystal waveguides in silicon.* Optics Express, 2012. **20**(28): p. 29361-29368.
14. Shankar, R., et al., *Mid-infrared photonic crystal cavities in silicon.* Optics Express, 2011. **19**(6): p. 5579-5586.
15. Mortensen, N.A. and S. Xiao, *Slow-light enhancement of Beer-Lambert-Bouguer absorption.* Applied Physics Letters, 2007. **90**(14): p. 141108.
16. Zou, Y., et al. *Silicon Chip Based Near-Infrared and Mid-Infrared Optical Spectroscopy for Volatile Organic Compound Sensing*. in *CLEO: Science and Innovations*. 2014. Optical Society of America.
17. Almeida, V.R., et al., *Guiding and confining light in void nanostructure.* Optics Letters, 2004. **29**(11): p. 1209-1211.
18. Notomi, M., et al., *Extremely large group-velocity dispersion of line-defect waveguides in photonic crystal slabs.* Physical Review Letters, 2001. **87**(25): p. 253902.
19. Lai, W.-C., et al. *Comparative sensitivity analysis of integrated optical waveguides for near-infrared volatile organic compounds with 1ppb detection*. in *SPIE OPTO*. 2014. International Society for Optics and Photonics.
20. Zou, Y., et al., *The role of group index engineering in series-connected photonic crystal microcavities for high density sensor microarrays.* Applied Physics Letters, 2014. **104**(14): p. 141103.
21. Zou, Y., et al., *Cavity-Waveguide Coupling Engineered High Sensitivity Silicon Photonic Crystal Microcavity Biosensors with High Yield*. 2014.
22. Frey, B.J., D.B. Leviton, and T.J. Madison. *Temperature-dependent refractive index of silicon and germanium*. in *Astronomical Telescopes and Instrumentation*. 2006. International Society for Optics and Photonics.